ISNN:2181-1296

SHAROF RASHIDOV NOMIDAGI
SAMARQAND DAVLAT UNIVERSITETI

САМАРКАНДСКИЙ ГОСУДАРСТВЕННЫЙ
УНИВЕРСИТЕТ ИМЕНИ ШАРОФА РАШИДОВА

SAMARKAND STATE UNIVERSITY NAMED
AFTER SHAROF RASHIDOV

ILMIY AXBOROTNOMA

НАУЧНЫЙ ВЕСТНИК
SCIENTIFIC JOURNAL

ANIQ VA TABIIY FANLAR SERIYASI

Matematika, Mexanika, Informatika
Fizika, Kimyo, Biologiya, Geografiya

№ 1/2 (155)
2026

ISSN 2181-1296

ILMIY AXBOROTNOMA

НАУЧНЫЙ ВЕСТНИК SCIENTIFIC JOURNAL

2026-yil, 1-son (155/2) ANIQ VA TABIIY FANLAR SERIYASI

Matematika, Mexanika, Informatika, Fizika, Kimyo, Biologiya, Geografiya

Samarqand viloyat matbuot boshqarmasida ro‘yxatdan o‘tish tartibi 09-25.
Jurnal 1999-yildan chop qilina boshlagan va OAK ro‘yxatiga kiritilgan.

BOSH MUHARRIR **R. I. XALMURADOV, t.f.d., professor**
BOSH MUHARRIR O‘RINBOSARLARI: **H.A. XUSHVAQTOV, f-m.f.d., dotsent**

TAHRIRIYAT KENGASHI:

Sh.A.Alimov	- O‘zFA akademigi	**M.X.Ashurov**	- O‘zFA akademigi
S.N.Lakayev	- O‘zFA akademigi (SamDU)	**B.J.Axmedov**	- O‘zFA akademigi
M.M.Kamilov	- O‘zFA akademigi	**Q.G‘.G‘ulomov**	- O‘zFA akademigi
A.G.Yagola	- Moskva davlat universiteti professori (Rossiya)	**A.A.Zaxidov**	-Texas Nanotexnologiya instituti professori (AQSh)
Alberto Del Bimbo	-Florensiya universiteti professori (Italiya)	**N.B. Ferapontov**	- Moskva davlat universiteti professori (Rossiya)
Sh.Tugizov	-Kaliforniya universiteti professori (AQSh)	**V.L.Popov**	-Berlin texnika universiteti professori (Germaniya)
A.S.Soleev	- f.-m.f.d., professor (SamDU)	**N.F.Bunkin**	- Moskva davlat texnika universiteti professori (Rossiya)
I.A.Ikromov	- f.-m.f.d., professor (SamDU)	**Haji Akber Aisa**	-Xinjiang tibbiyot universiteti professori (Xitoy)
B.X.Xo‘jayarov	- f.-m.f.d., professor (SamDU)	**E. A. Abduraxmonov**	- k.f.d., professor (SamDU)
L.Sabirov	-f.-m.f.d., professor (SamDU)	**N. K. Muxamadiyev**	- k.f.d., professor (SamDU)
A.Jumaboyev	-f.-m.f.d., professor (SamDU)	**L. A. Bulavin**	- Kiev milliy universiteti
X.Bozorov	-k.f.d., professor (SamDU)	**X. Q. Xaydarov**	- b.f.d., professor (SamDU)
O.Q.Quvondiqov	-f.-m.f.d. professor (SamDU)	**Z. I. Izzatullayev**	- b.f.d., professor (SamDU)
A.Z.Xasanov	-f.-m.f.d. professor (SamDU)	**A.B.Hasanov**	-tex.f.d., professor (SamDU)
Muhammad Suzuri bin Hitam	- Terengganu universiteti professori (Malayziya)	**Sh. T. Xoliqulov**	- q.-x.f.d., professor (SamDU)
K.D.Kuliyev	- f.-m.f .n. professor (SamDU)	**S. B. Abbosov**	- g.f.d., professor (SamDU)
A.M.Xolxo‘jayev	-f.-m.f.d., professor (SamDU)	**M.E. Mo‘minov**	-f.-m.f.d., professor (SamDU)
J.Abdullayev	-f.-m.f.d., professor (SamDU)	**I.I.Jumanov**	-tex.f.d., professor (SamDU)
A.R.Axatov	-tex.f.d., professor (SamDU)	**N.S.Mamatov**	-tex.f.d., professor (TIQXMMI)
D.B.Xursanov	- g.f.f.d., dotsent (SamDU)	**A.Sh.Yarmuxamedov**	-f-m.f.n., dotsent (SamDU)
F.Nazarov	-tex.f.d., dotsent (SamDU)	**X.S.Xaydarov**	-f-m.f.n., dotsent (SamDU)

Obuna indeksi – yakka tartibdagi obunachilar uchun **- 5583,**
tashkilot, korxonalar uchun **- 5584**

M U N D A R I J A
C O N T E N T S

№	Maqola nomi	Article title	Bet/ page
1.	Yuqori chastotali II-turdagi radio portlash spektral kuzatuvlaridan foydalanib magnit maydon kuchini baholash **Pulatov D., Mirtoshev Z.**	Estimation Of The Coronal Magnetic Field Strength Using High-Frequency Type Ii Radio Burst Observations **Pulatov D., Mirtoshev Z.**	**5-11**
2.	Rayxon (OCIMUM) o‘simligi efir moyi kimyoviy tarkibiga iqlim omillarining ta’sirini GX–MS usulida tadqiq etish **Siddikova Y., Saifullaeva Sh., Mukhamadiyev A., N.Fazlieva, Nayimova B., Muhamadiyev N.**	Study of the influence of climate factors on the chemical composition of basil (ocimum) essential oil using the GH–MS method **Siddikova Y., Saifullaeva Sh., Mukhamadiev A., N.Fazlieva, Nayimova B., Muhamadiev N.**	**12-20**
3.	Bentonitni montmorillonit bilan boyitishning samarali usullari va termal ishlov berishning kation almashinuvi quvvatiga ta'siri **Mamadoliev I., Abdikamalova A., Ruzieva S.**	Effective methods for bentonite enrichment with montmorillonite and the impact of thermal treatment on cation exchange capacity **Mamadoliev I., Abdikamalova A., Ruzieva S.**	**21-28**
4.	$KPbBr_3$ asosidagi peroled tuzilmalarida zaryad tashish mexanizmlari va energetik sathlarning moslashuvi **Rahmonova M., Muxamadiyev N.**	Charge transport mechanisms and energy level alignment in $KPbBr_3$ -based peroled structures **Rahmonova M., Mukhamadiev N.**	**29-36**
5.	*N*-(4-(((7-Nitroxinazolin-4-il) amino) metil)fenil) siklogeksankarboksamid sintezi **Gaybullaev Sh., Takhirov Y., Chao Niu, Bozorov Kh.**	Synthesis of N-(4-(((7-nitroquinazolin-4-YL) amino) methyl) phenyl) cyclohexanecarboxamide **Gaybullaev Sh., Takhirov Y., Chao Niu, Bozorov Kh.**	**37-41**
6.	3-brom-pirido[2,3-*d*]pirimidinonlarning sintezi **Khushnazarov Z., Turgunov D., Bozorov Kh.**	synthesis of 3-bromo-pyrido[2,3-d]pyrimidinones **Khushnazarov Z., Turgunov D., Bozorov Kh.**	**42-46**
7.	Zarrachalar tezlatkichlarida materiallarning aktivatsiyasi va radiatsion xavflar **Temirov J., Khasanov Sh., Safarov A., Karimberganova Q.**	Material activation and radiological hazards in particle accelerators **Temirov J., Khasanov Sh., Safarov A., Karimberganova Q.**	**47-57**
8.	Geoinformatsion dasturlar yordamida demografik atlaslar yaratishning afzalliklariga nazar **Tukhtamishev Sh., Khudoyarova Sh., Shirinboyev D.**	Advantages of creating demographic atlases using geoinformation software **Tukhtamishev Sh., Khudoyarova Sh., Shirinboev D.**	**58-62**
9.	Siklopropilatsetilen asosida atsetilen spirtlari sintezi, ularning nazariy energetik xarakteristikalari va nadfoksidaza oqsili (7U8G) bilan molekulyar birikish tahlili **Ziyadullaev M.E., Nurmanov S.E., Buriev F.Kh., Abdukhalikov F.J.**	Synthesis of acetylenic alcohols based on cyclopropylacetylene, their theoretical energetic characterization, and molecular docking analysis with nadph oxidase (7U8G) protein **Ziyadullaev M.E., Nurmanov S.E., Buriev F.Kh., Abdukhalikov F.J.**	**63-71**
10.	Tetratsiklik tieno[3,2-*d*]pirimidinonlarning siklooksigenaza-2 ingibitorlari sifatida *in silico* tadqiqi **Nasrullaev A., Buronov A., Gaybullaev Sh., Bozorov Kh.**	In silico evaluation of tetracyclic thieno[3,2-d]pyrimidinones as potential cyclooxygenase-2 inhibitors **Nasrullaev A., Buronov A., Gaybullaev Sh., Bozorov Kh.**	**72-76**
11.	H3PO4, KOH va ZnCl2 yordamida olingan faollashtirilgan ko‘mirning morfologik va strukturaviy xususiyatlarining qiyosiy tahlili **Ergasheva D., Mukhamadiyev A., Mukhamadiyev N., Uzokov J.**	Comparative analysis of the morphological and structural properties of activated carbon prepared using H_3PO_4, KOH, and $ZnCl_2$ **Ergasheva D., Mukhamadiev A., Mukhamadiev N., Uzokov J.**	**77-81**
12.	CO_2 NI quyosh nuri ta’sirida samarali konversiyalashni ta’minlovchi g-C_3N_4/$CoNi_2S_4$ geterotuzilmali nanomateriallar sintezi va fizik-kimyoviy xossalari **Samiev A., Nizamov U.N., Mirzaev Sh., Ruzimuradov O., Nasimov A.**	Synthesis and physicochemical properties of γ-C3N4/CoNi2S4 heterostructured anomaterials providing efficient conversion of CO2 under the influence of sunlight **Samiev A., Nizamov U.N., Mirzaev Sh., Ruzimuradov O., Nasimov A.**	**82-87**

№	Maqola nomi	Article title	Bet/ page
13.	Atrof muhitdagi ammiak mikrokensentratsiyasini monigitori uchun gibrid perovskit $MA_xFA_{1-x}PbI_3$ fluoressent sensori tayyorlash **Eshmuradova G.B., Tashpulatov Kh.Sh., Khursandov J.M., Normuradov O.U., Norboyev Q.M., Toshpulatov D.T.**	Preparation of hybride perovskite $MA_xFA_{1-x}PbI_3$-fluorescent sensor for the monitoring of ammonia microconcentration in environment **Eshmuradova G.B., Tashpulatov Kh.Sh., Khursandov J.M., Normuradov O.U., Norboev Q.M., Toshpulatov D.T.**	**88-92**
14.	Al^{3+} bilan modifikatsiyalangan shpinel tuzilishga ega $Li_{1.33}Al_XMn_{1.67-X}O_4$ ($0 \leq x < 0.7$) tarkibli adsorbentlarning zol-gel sintezi va fizik-kimyoviy xossalari **Begimkulova Sh.A., Nematova Sh.Sh., Baxriev I.S., Mirzaev Sh.E., Ruzimuradov O.N., Nasimov A.M.**	Sol-gel synthesis and physicochemical properties of adsorbents consisting of Al^{3+} modified spinel structure $LI_{1.33}Al_XMn_{1.67-X}O_4$ ($0 \leq X < 0.7$) **Begimkulova Sh.A., Nematova Sh.Sh., Baxriev I.S., Mirzaev Sh.E., Ruzimuradov O.N., Nasimov A.M.**	**93-99**
15.	CdCr2Se4 va CuCr4Se4 magnitli yarimo‘tkazgichda magnit-optik effektlar **Dosmurodov G.**, **Kurbaniyazov A.**, **Boboqambarova G.**	Magneto-optical effects in the magnetic semiconductor CdCr2Se4 AND CuCr4Se4 **Dosmurodov G.**, **Kurbaniyazov A.**, **Bobokambarova G.**	**100-104**
16.	Sophora lehmanni va Cicer mogoltavikum o‘simliklari yer ustki qismilarining flavonoidlari **Gafurov A.Zh, Botirov E. Kh.**	Flavonoids of aerial parts of sophora lehmannii and cicer mogoltavicum **Gafurov A.Zh, Botirov E. Kh.**	**105-109**
17.	Buxoro viloyatining balneologik resurslari va ularning aholi salomatligini yaxshilashdagi ahamiyati **Zaynutdinova D.K., Nematova Kh. Kh.**	Balneological resources of the bukhara region and their significance in improving public health **Zaynutdinova D.K., Nematova Kh. Kh.**	**110-116**
18.	Tabiiy cho‘kuvchan gruntlarni polimer-kompozitsion eritmalar bilan inyeksion mustahkamlash texnologiyasini matematik rejalashtirish **Bakhriyev N.F., Kholiqulov O.O., Nurmatova R.K.**	Mathematical planning of injection strengthening technology of natural collapsible soils using polymer-composite solutions **Bakhriyev N.F., Kholikulov O.O., Nurmatova R.K.**	**117-125**
19.	Adgezion kontaktlarda ishqalanish koeffitsiyentiga geometrik parametrlar hamda tashqi yuk ta’sirining tahlili **Bekmamatova G., Xoliqulov O., Tojinorov M.**	Analysis of geometric parameters and external load on the friction coefficient in adhesive contacts **Bekmamatova G., Xolikulov O., Tojinorov M.**	**126-131**
20.	Markaziy Osiyo iqlim sharoitida sorbsion sovutgichlardan biogaz komplekslari bilan simbiozda foydalanish istiqbollari **Abdusamiyev F., Bahriev S., Sattarov S.**	Prospects for using sorption refrigerators in symbiosis with biogas complexes in the climatic conditions of Central Asia **Abdusamiev F., Bahriev S., Sattarov S.**	**132-136**
21.	Maple tizimida algebraik ko’pxilliklarni ratsional parametrlashining nazariy asoslari va kompyuterda amalga oshirilishi **Usmonova N.**	Theoretical foundations and computer implementation of rational parameterization of algebraic manifolds in the maple system **Usmonova N.**	**137-142**
22.	$Fe_5Ga_6Gd_2YZr$ ko‘p komponentli kristallining element tarkibi va tebranish xossalarini rentgen-fluoresans (XRF) va raman spektroskopiyasi yordamida tadqiq etish **Nasirova N., Fayziyev Sh., Saidov Q., Qaxorova Sh., Sharipov M., Djuraev D.**	Investigation of the elemental composition and vibrational properties of the multicomponent crystal Fe5Ga6Gd2YZr using X-RAY fluorescence (XRF) and raman spectroscopy **Nasirova N., Fayziyev Sh., Saidov Q., Qaxorova Sh., Sharipov M., Djuraev D.**	**143-152**
23.	Xofp tipidagi tenglamalar sistemasi uchun Koshi masalasi **Erkinova D. A.**, **Imomnazarov Kh. Kh.**	Cauchy problem for a Hopf-type system **Erkinova D. A.**, **Imomnazarov Kh. Kh.**	**153-157**
24.	Ar va HCl izotopologlari o‘rtasida hosil bo‘lgan komplekslarning kvant-kimyoviy tahlili: AIM, RDG va NCI usullari yordamida solvatatsiya effektlarini o‘rganish **Khujamov U.**	Quantum-chemical analysis of complexes formed between Ar and HCL isotopologues: studying solvation effects using AIM, RDG, and NCI methods **Khujamov U.**	**158-167**

UDC: 539.163:504.069 https://doi.org/10.59251/2181-3973.2025.v1.138.1.3771

MATERIAL ACTIVATION AND RADIOLOGICAL HAZARDS IN PARTICLE ACCELERATORS

J.Temirov, Sh.Khasanov, A.Safarov, Q.Karimberganova
Samarkand State University named after Sharof Rashidov, Samarkand, Uzbekistan.

J.Temirov Samarkand State University named after Sharof Rashidov, Samarkand, Uzbekistan.

Received: 15.01.2026
Revised: 30.01.2026
Accepted: 14.02.2026
Published: 30.03.2026

Publisher: Samarkand State University named after Sharof Rashidov.

Abstract. Particle accelerators used in research, medicine, and industry generate secondary radiation fields that induce radioactivity in structural components, shielding materials, coolant systems, air, soil, and groundwater. Understanding the production mechanisms, radionuclide inventories, and radiological consequences of induced radioactivity is essential for facility design, personnel dose management, environmental protection, and decommissioning planning. The current work provides a comprehensive analysis of the principal sources of induced radioactivity at modern accelerator facilities, covering the relevant nuclear reaction channels (thermal neutron capture, threshold reactions, and spallation), key radionuclides and their half-lives, saturation and decay kinetics, depth-dependent activation profiles in shielding, environmental migration pathways, and state-of-the-art Monte Carlo simulation approaches. Updated data from FLUKA, PHITS, MCNP, and Geant4 studies at major facilities worldwide are synthesized. The paper is intended to serve as a reference for accelerator physicists, radiation protection officers, medical physicists, and environmental scientists.

Keywords: induced radioactivity, particle accelerators, neutron activation, radiation protection, Monte Carlo.

Zarrachalar tezlatkichlarida materiallarning aktivatsiyasi va radiatsion xavflar

Annotatsiya. Ilmiy tadqiqotlar, tibbiyot va sanoatda qo‘llaniladigan zarrachalar tezlatkichlari ikkilamchi nurlanish maydonlarini hosil qiladi, bu esa konstruktiv elementlar, himoya materiallari, sovitish tizimlari, havo, tuproq va yer osti suvlarida induksiyalangan (qoldiqli) radioaktivlikni yuzaga keltiradi. Induksiyalangan radioaktivlikning hosil bo‘lish mexanizmlari, radionuklidlar tarkibi va radiatsion oqibatlarini tushunish obyektlarni loyihalash, xodimlarning dozaviy yuklamasini boshqarish, atrof-muhitni muhofaza qilish hamda ekspluatatsiyadan chiqarishni rejalashtirish uchun muhim ahamiyatga ega. Mazkur maqolada zamonaviy tezlatkich majmualarida induksiyalangan radioaktivlikning asosiy manbalari kompleks tahlil qilinadi. Unda tegishli yadro reaksiyalari kanallari (issiqlik neytronlarini tutib olish, chegaraviy reaksiyalar va spallatsiya), asosiy radionuklidlar va ularning yarim yemirilish davrlari, to‘yinish va parchalanish kinetikasi, himoya materiallarida chuqurlik bo‘yicha aktivatsiya profillari, atrof-muhitda migratsiya yo‘llari hamda zamonaviy Monte-Karlo modellashtirish usullari ko‘rib chiqiladi. Dunyoning yirik tezlatkich obyektlarida FLUKA, PHITS, MCNP va Geant4

dasturlari yordamida olingan yangilangan ma’lumotlar umumlashtirilgan.

Kalit so‘zlar: induksiyalangan radioaktivlik, zarrachalar tezlatkichlari, neytron aktivatsiyasi, radiatsion himoya, Monte-Karlo.

Активация материалов и радиационные опасности на ускорителях частиц

Аннотация. Ускорители частиц, применяемые в научных исследованиях, медицине и промышленности, формируют вторичные поля излучения, которые вызывают наведённую радиоактивность в конструкционных элементах, защитных материалах, системах охлаждения, воздухе, почве и подземных водах. Понимание механизмов образования радионуклидов, их номенклатуры и радиационных последствий наведённой радиоактивности имеет принципиальное значение для проектирования установок, управления дозовыми нагрузками персонала, обеспечения охраны окружающей среды и планирования вывода объектов из эксплуатации. В настоящей работе представлен комплексный анализ основных источников наведённой радиоактивности на современных ускорительных установках, включая соответствующие каналы ядерных реакций (захват тепловых нейтронов, пороговые реакции и спалляция), ключевые радионуклиды и их периоды полураспада, кинетику насыщения и распада, глубинные профили активации в защитных материалах, пути миграции в окружающей среде, а также современные методы моделирования Монте-Карло. Обобщены актуальные данные расчётов с использованием кодов FLUKA, PHITS, MCNP и Geant4, полученные на ведущих ускорительных комплексах мира.

Ключевые слова: наведённая радиоактивность, ускорители частиц, нейтронная активация, радиационная защита, Монте-Карло.

Introduction. When the kinetic energy of accelerated particles exceeds approximately 10 MeV per nucleon, the probability of nuclear reactions with the materials in their path increases dramatically [1,2]. At modern accelerator facilities—ranging from multi-GeV synchrotrons at CERN and Fermilab to clinical proton- and carbon-ion therapy centers—beam losses on aperture-limiting devices, targets, beam dumps, and other components produce intense secondary radiation fields dominated by neutrons, protons, pions, and photons. These secondary particles, in turn, undergo further nuclear interactions with surrounding materials, generating a wide spectrum of radioactive isotopes through various reaction channels.

The resulting *induced radioactivity* is a central concern in radiation protection and has implications for: (i) occupational doses to personnel during maintenance, (ii) environmental releases through activated air and water, (iii) waste management and disposal classification, and (iv) decommissioning costs and timelines. Over the past two decades, the increasing beam intensities at high-energy physics laboratories, the rapid proliferation of medical accelerators, and the planned construction of next-generation facilities such as the European Spallation Source (ESS), the Facility for Antiproton and Ion Research (FAIR), and the International Linear Collider (ILC) have driven renewed interest in accurate prediction and minimization of induced radioactivity [3–5].

This review presents a systematic analysis of the sources of induced radioactivity at particle accelerator facilities. It extends and updates previous treatments [1,6,7] by incorporating recent Monte Carlo simulation results, new experimental data from operating facilities, and relevant dosimetric frameworks. The paper is organized as follows: Section 2 describes the fundamental physics of radionuclide production; Section 3 discusses activation of accelerator structural materials; Section 4 covers concrete and other shielding materials; Section 5 addresses cooling water; Section 6 treats air activation; Section 7 examines soil and groundwater; Section 8 reviews computational methods; and Section 9 discusses mitigation strategies and decommissioning. A concluding summary and outlook are provided in Section 10.

Fundamental physics of radionuclide production. Induced radioactivity at accelerator facilities arises from several categories of nuclear reactions, each dominant in a characteristic energy regime [1,8]:

Thermal neutron capture reactions (n,γ) occur predominantly at neutron energies below approximately 0.5 eV. In this energy range, many isotopes exhibit relatively high capture cross-sections, resulting in efficient activation under thermal neutron flux. Examples include ^{23}Na (σ_{th} = 0.53 b), ^{59}Co (σ_{th} = 37.2 b), and ^{151}Eu (σ_{th} = 9200 b). This mechanism is particularly important in concrete shielding, where thermalized neutrons can travel significant distances before capture.

Threshold reactions: Above characteristic energy thresholds (typically 1–20 MeV), reactions such as (n,p), (n,α), (n,2n), and (p,n) become energetically allowed. These produce radionuclides that are generally neutron-deficient relative to the target, and their cross-sections peak at energies of several to tens of MeV before decreasing. Examples include ^{63}Cu(n,2n)^{62}Cu (threshold ~11 MeV) and ^{56}Fe(p,n)^{56}Co [9] (see Figure 1).

Spallation: At energies above ~100 MeV, high-energy nucleons initiate intranuclear cascades in which multiple nucleons and light fragments are ejected from the target nucleus. This process produces a broad distribution of product nuclides with mass numbers ranging from near that of the target down to very light species (^{3}H, ^{7}Be). Spallation is the dominant mechanism for activation by high-energy neutrons at proton and heavy-ion accelerator facilities [1,10].

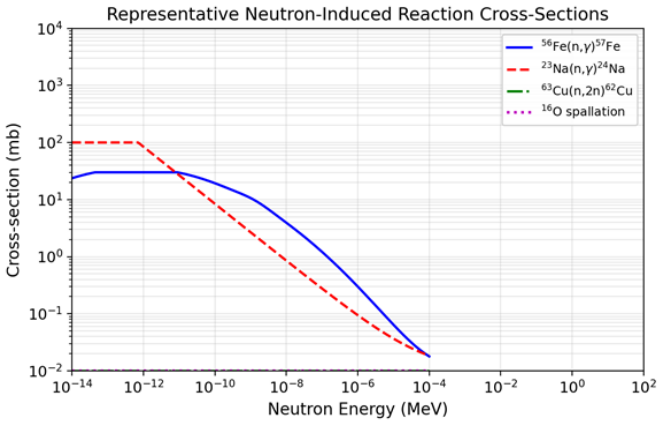


Figure 1. Representative energy dependence of neutron-induced reaction cross-sections for key materials found at accelerator facilities.

Activation equation and saturation activity. The activity A(t) of a radionuclide produced by a constant flux of particles during an irradiation of duration t_{irr} is governed by the fundamental activation equation [1,6]:

$$A(t_{irr}) = N \cdot \sigma \cdot \Phi \cdot (1 - e^{(-\lambda t irr)})$$

where N is the number of target atoms, σ is the production cross-section (cm^2), Φ is the particle flux (cm^{-2} s^{-1}), and $\lambda = \ln(2)/T_{1/2}$ is the decay constant of the product nuclide. The quantity $A_{sat} = N\sigma\Phi$ is the saturation activity, approached when $t_{irr} >> T_{1/2}$. For short-lived nuclides, saturation is reached rapidly; for long-lived species, the activity builds up quasi-linearly with time (see Figure 2).

After irradiation ceases, the residual activity decays exponentially:

$$A(t_{cool}) = A(t_{irr}) \cdot e^{-\lambda t cool}$$

where t_{cool} is the cooling time after the end of irradiation. For a mixture of radionuclides, the total activity is the sum of individual contributions. The effective dose rate at a point of interest is obtained by further considering the emission spectra, self-shielding, and geometry:

$$\dot{H}(r, t_{cool}) = \Sigma_i A_i(t_{cool}) \cdot \Gamma_i \cdot G(r)$$

where Γ_i is the specific gamma-ray dose constant ($Sv \cdot m^2 \cdot MBq^{-1} \cdot h^{-1}$) and G(r) is a geometry factor including distance and attenuation corrections.

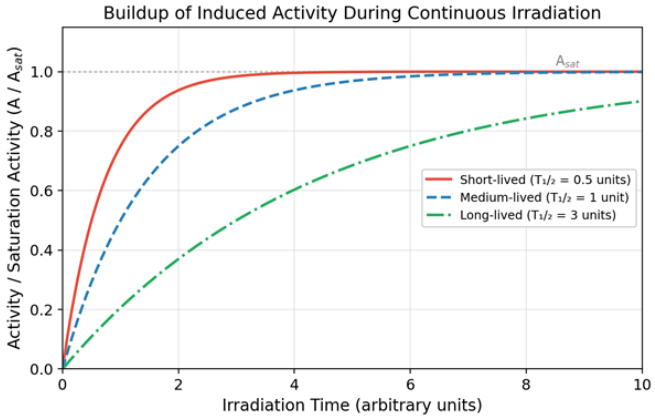


Figure 2. Buildup of induced activity toward saturation for radionuclides with different half-lives during continuous irradiation.

Key parameters governing activation. The degree of activation depends on several factors: (i) the particle type and energy spectrum; (ii) the elemental composition of the irradiated material; (iii) the irradiation time relative to the product half-life; (iv) the magnitude of the particle flux; and (v) the spatial distribution of the secondary field. Materials with higher atomic number Z generally yield a larger variety of activation products because more reaction channels are energetically accessible [1,2].

Beam losses at aperture restrictions, collimators, septa, targets, and beam dumps initiate hadronic cascades that produce intense local radiation fields. The principal structural materials—copper, iron and steel, aluminum alloys, and graphite—become activated to varying degrees depending on the beam parameters and proximity to loss points [1,2,11].

Table 1 summarizes the key radionuclides produced in common accelerator construction materials via proton- and neutron-induced reactions, considering only those with half-lives between 10 minutes and 5 years. Pure β^- emitters are excluded because their radiation is substantially self-shielded by the bulk material. However, pure β^+ emitters such as ^{11}C produce 511 keV annihilation photons upon positron–electron interaction, contributing to the ambient dose rate [2].

Table 1. Principal radionuclides produced in accelerator structural materials [1,2,9,11].

Material	Radionuclide	Half-life	Primary Reaction	E_γ (keV)
Graphite	^{3}H	12.33 y	$^{12}C(n,t)$	β^+ only
	^{7}Be	53.12 d	$^{12}C(n,spall)$	478
	^{11}C	20.39 min	$^{12}C(n,2n)$	511 (ann.)
Aluminum	^{22}Na	2.60 y	$^{27}Al(n,spall)$	1275
	^{24}Na	14.96 h	$^{27}Al(n,\alpha)$	1369, 2754
	^{18}F	109.8 min	$^{27}Al(p,x)$	511 (ann.)
Iron	^{54}Mn	312.3 d	$^{56}Fe(n,t)$	835
	^{56}Co	77.27 d	$^{56}Fe(p,n)$	847, 1238
	^{57}Co	271.8 d	$^{58}Fe(n,2n)$ / spall	122, 136

	^{58}Co	70.86 d	^{58}Ni(n,p)	811
	^{51}Cr	27.70 d	^{52}Cr(n,2n)	320
	^{46}Sc	83.79 d	^{46}Ti(n,p) / spall	889, 1121
	^{48}V	15.97 d	^{51}V(n,α)	984, 1312
Stainless steel	^{60}Co	5.27 y	^{59}Co(n,γ)	1173, 1332
	^{57}Ni	35.6 h	^{58}Ni(n,2n)	127, 1378
Copper	^{64}Cu	12.70 h	^{63}Cu(n,γ)	511 (ann.)
	^{65}Zn	244.3 d	^{65}Cu(n,p)	1116
	^{62}Zn	9.19 h	^{63}Cu(n,2n)	548, 597
	^{61}Cu	3.33 h	^{63}Cu(n,3n) / spall	283, 656

The choice of structural material directly impacts the residual dose rates and cooling times required before personnel access. Graphite is preferred for patient positioning tables in therapy rooms because ^{11}C ($T_{1/2}$ = 20.4 min) decays to negligible levels within ~3 hours. Copper and iron/steel components generate longer-lived species (^{65}Zn, ^{54}Mn, ^{60}Co) that may persist for months to years, dominating residual dose rates during shutdowns [11,12] (see Figure 3).

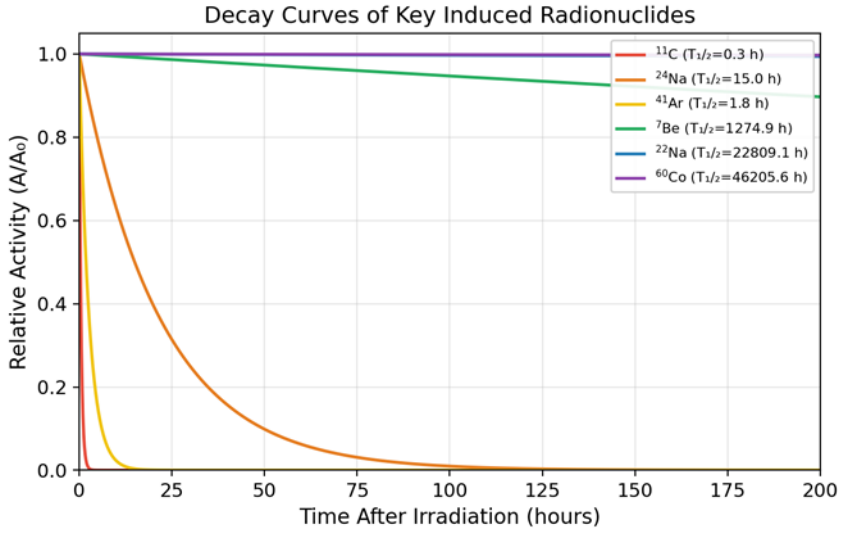


Figure 3. Decay curves of principal induced radionuclides following shutdown of a particle accelerator.

Residual dose rate estimation. The ambient dose equivalent rate H*(10) at a distance d from an activated component after cooling time t_{cool} can be estimated using the omega factor approach [13]:

$$\dot{H}^*(10) = \Omega(E_p, t_{irr}, t_{cool}) \cdot P_{beam} / d^2$$

where Ω is the material- and energy-dependent omega factor (Sv·m^2/proton), E_p is the primary beam energy, and P_{beam} is the integrated number of lost protons per unit length. The omega factors have been extensively tabulated for copper, iron, and concrete through FLUKA and MARS simulations by Huhtinen [13] and Sullivan [14]. For a typical copper target after 30 days of irradiation at 1 GeV and 1 day of cooling, $\Omega \approx 3 \times 10^{-15}$ Sv·m^2/proton.

Activation of concrete shielding. Concrete is the primary shielding material at most accelerator facilities because of its favorable cost, structural properties, and neutron attenuation characteristics. Although direct beam impact on concrete is uncommon, the intense secondary neutron fields—spanning from thermal energies to hundreds of MeV—produce a complex mixture of radionuclides through the entire depth of the shield [1,15,16].

The activation products in concrete can be classified by production mechanism:

(i) Thermal neutron capture products: ^{24}Na (from ^{23}Na, σ_{th} = 0.53 b, $T_{1/2}$ = 14.96 h), ^{152}Eu (from ^{151}Eu, σ_{th} = 9200 b, $T_{1/2}$ = 13.5 y), and ^{60}Co (from ^{59}Co, σ_{th} = 37.2 b, $T_{1/2}$ = 5.27 y). These species are produced primarily at greater depths in the shield where the neutron spectrum has been thermalized.

(ii) Spallation products: ^{22}Na, ^{7}Be, ^{3}H, and ^{54}Mn, produced by high-energy neutrons (E > 100 MeV) predominantly in the first 30–50 cm of the shield where the high-energy flux is highest.

Table 2 provides updated data on long-term activation products in concrete, including results from Zhang et al. [16], Oishi et al. [17], and FLUKA simulations at CERN [18].

Table 2. Long-lived radionuclides in activated concrete shielding [15–19].

Nuclide	Half-life	Target Element	Reaction Type	Dose Contribution
^{3}H	12.33 y	O, Si, Ca	Spallation	Negligible (β only)
^{7}Be	53.12 d	O, Si	Spallation	Low
^{22}Na	2.60 y	Na, Si, Al	Spallation	Moderate
^{46}Sc	83.79 d	Ca, Fe	Spallation / (n,p)	Moderate
^{54}Mn	312.3 d	Fe	Spallation / (n,p)	Significant
^{60}Co	5.27 y	Co (trace)	(n,γ)	Significant
^{134}Cs	2.06 y	Ba (trace)	(n,γ)	Significant
^{152}Eu	13.5 y	Eu (trace)	(n,γ)	Dominant (long-term)
^{154}Eu	8.59 y	Eu (trace)	(n,γ)	Dominant (long-term)
^{45}Ca	162.6 d	Ca	(n,γ) / spall	Low
^{36}Cl	3.01×10^{5} y	Cl (trace)	(n,γ)	Very long-term

Zhang et al. [16] measured the activation of a 200 cm-thick concrete shield surrounding a proton cyclotron and found that ^{154}Eu, ^{152}Eu, ^{134}Cs, and ^{60}Co together account for 99.9% of the long-term residual dose. This finding is consistent with decommissioning studies at other facilities and underscores the importance of trace element composition (especially europium and cobalt) in concrete for waste classification [15,18].

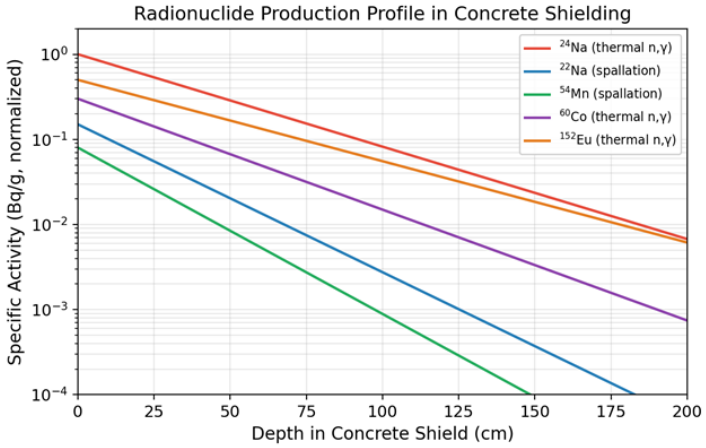


Figure 4. Depth profile of specific activity for key radionuclides in a concrete shield. Thermal capture products extend deeper than spallation products.

Reducing the trace content of Na, Co, Eu, Cs, and Ba in concrete aggregates can substantially lower the long-term residual activity and simplify decommissioning (see Figure 4). Several facilities, including J-PARC and ESS, have specified low-activation concrete formulations

using serpentinite or magnetite aggregates with controlled trace element content [19,20]. Studies show that the dose rate from activated concrete 5 years after shutdown can be reduced by an order of magnitude through judicious aggregate selection [18].

Activation of cooling water. The cooling water circulating through targets, magnets, and beam dumps is subject to activation primarily through spallation reactions on ^{16}O nuclei by high-energy neutrons [1,21]. The principal radionuclides produced are:

Table 3. Radionuclides produced in cooling water via spallation of ^{16}O [1,21,22].

Radionuclide	Half-life	Decay Mode	Remarks
^{15}O	122.2 s	β^+, γ (511 keV ann.)	Short-lived; decays in-pipe
^{13}N	9.97 min	β^+, γ (511 keV ann.)	Gaseous; may escape to air
^{11}C	20.39 min	β^+, γ (511 keV ann.)	Gaseous; desorbs from water
^{7}Be	53.12 d	EC, γ (478 keV)	Removed by ion-exchange resins
^{3}H	12.33 y	β^- (18.6 keV max)	Cannot be removed chemically

Among these, only ^{3}H (tritium) and ^{7}Be have half-lives long enough to accumulate to operationally significant levels. ^{7}Be is effectively removed by mixed-bed ion-exchange resins during water circulation, leaving tritium as the sole long-lived contaminant requiring continuous monitoring [21]. Tritium cannot be separated from water by conventional treatment and builds up in closed-loop systems, necessitating periodic dilution or controlled release.

Yang [22] demonstrated through both static and dynamic modeling that the equilibrium total activity in a cooling system is independent of flow conditions; however, the spatial distribution of activity along the circuit changes. Under flowing conditions, long-lived species become uniformly distributed throughout the pipework, while short-lived species are concentrated near the activation zone. This has implications for shielding design of pump rooms and heat exchangers.

Activation of air. Air within and near accelerator enclosures interacts with both primary and secondary radiation fields, producing a suite of radionuclides that contribute to both internal (inhalation) and external (immersion) doses. Adequate ventilation is critical to maintain concentrations below regulatory limits [1,23].

Table 4 presents the principal airborne radionuclides observed at accelerator facilities, adapted and updated from Swanson and Thomas [23] with data from Butala et al. [24] and recent FLUKA calculations for the CERN accelerator complex [25]. The production mechanisms include spallation of nitrogen and oxygen nuclei, thermal neutron capture by ^{40}Ar (producing ^{41}Ar), and photonuclear reactions.

Table 4. Radionuclides produced in air at particle accelerator facilities [1,23–25].

Nuclide	Half-life	Parent nuclide	Reaction	σ (mb)
^{3}H	12.33 y	N, O	Spallation	30
^{7}Be	53.12 d	N, O, Ar	Spallation	10 / 5 / 0.6
^{11}C	20.39 min	N, O, Ar	Spallation	10 / 0.7 / 0.7
^{14}C	5730 y	N	(n,p) thermal	1640
^{13}N	9.97 min	N, O, Ar	Spallation / (γ,n)	10 / 9 / 0.8
^{15}O	122.2 s	O, Ar	Spallation / (γ,n)	40 / —
^{18}F	109.8 min	Ar	Spallation	6
^{22}Na	2.60 y	Ar	Spallation	10
^{24}Na	14.96 h	Ar	Spallation	7
^{32}P	14.26 d	Ar	Spallation	25
^{35}S	87.32 d	Ar	Spallation	23

^{38}Cl	37.24 min	Ar	(γ,pn)	4
^{39}Cl	55.6 min	Ar	(γ,p)	7
^{41}Ar	1.83 h	Ar	(n,γ) thermal	660

Dosimetric classification of airborne radionuclides.

The radiological impact of airborne radionuclides depends on their physical and chemical form, which determines their behavior in the respiratory tract. Following the ICRP Human Respiratory Tract Model [26], inhaled gases are classified as:

SR-0 (insoluble/inert): Noble gases and chemically inert species ($^{13}N_2$, $^{15}O_2$, ^{41}Ar) that are not deposited in the respiratory tract and contribute only to external immersion dose.

SR-1 and SR-2 (soluble): Reactive or soluble gases that deposit in the respiratory epithelium and may enter the bloodstream, contributing to organ doses. These include oxidized forms such as ^{11}CO, $^{11}CO_2$, and ^{3}HHO.

For noble gas nuclides (^{41}Ar, ^{37}Ar), the inhalation dose is negligible and only external immersion contributes to the effective dose. Furthermore, if the radiation emitted by a gaseous radionuclide cannot penetrate to the basal layer of the skin (~70 μm), the external immersion dose is also negligible [26,27].

Activation of soil and groundwater.

Many accelerator facilities are constructed underground, and the high-energy neutron fields that escape the concrete shielding can activate the surrounding geological media. This is an environmental concern because soluble activation products may migrate through soil to groundwater aquifers, potentially reaching drinking water supplies [28–31].

Radiochemical analyses of soil samples near high-energy accelerators have consistently identified ^{3}H, ^{7}Be, ^{22}Na, ^{45}Ca, ^{46}Sc, ^{48}V, ^{51}Cr, ^{54}Mn, ^{55}Fe, ^{59}Fe, and ^{60}Co as the principal products [28,30]. Borak et al. [28] at Fermilab, Miura et al. [30] at KEK, and Rokni et al. [29] at SLAC have independently confirmed this inventory using different experimental and computational methods.

Not all activation products are equally mobile in the subsurface. The migration behavior is controlled by solubility, distribution coefficient (K_d), and hydrological conditions. Table 5 summarizes the leaching and migration characteristics based on data from Borak et al. [28] and Baker et al. [32].

Table 5. Migration characteristics of key radionuclides in soil and groundwater [28,29,32].

Nuclide	Half-life	Solubility	Migration Rate	Risk Assessment
^{3}H	12.33 y	Complete	Equal to water velocity	High priority
^{22}Na	2.60 y	10–20% rapid	~40% of water velocity	Moderate priority
^{45}Ca	162.6 d	≤5%	Strongly adsorbed	Low priority
^{54}Mn	312.3 d	<2%	~90% soil-bound	Low priority
^{7}Be	53.12 d	Very low	Nearly immobile	Negligible
^{60}Co	5.27 y	Low	Strongly adsorbed	Low priority

Tritium migrates at the same velocity as groundwater because it exists as tritiated water (HTO) and is not retarded by soil sorption. ^{22}Na is partially soluble (10–20% dissolves rapidly), with a retardation factor of approximately 2.5 relative to water flow. The remaining species—^{45}Ca, ^{54}Mn, ^{7}Be, and ^{60}Co—are strongly adsorbed onto soil particles and pose minimal risk of groundwater contamination [28,32].

Consequently, ^{3}H and ^{22}Na are the only radionuclides requiring dedicated environmental monitoring programs at accelerator facilities. Regulatory limits for these nuclides in groundwater (typically 740 Bq/L for ^{3}H in the U.S. under DOE Order 5400.5) serve as the design criteria for shielding thickness [29,33].

Computational methods.

Monte Carlo radiation transport codes have become indispensable for predicting induced radioactivity, replacing earlier analytical and semi-empirical approaches [34–37]. The principal codes used worldwide are summarized in Table 6.

Table 6. Principal Monte Carlo codes for induced radioactivity calculations [34–38].

Code	Developer	Energy Range	Activation	Key Applications
FLUKA	CERN/INFN	0–PeV	Built-in	CERN, ESS, FAIR
PHITS	JAEA (Japan)	0–200 GeV	DCHAIN-SP	J-PARC, HIMAC
MCNP6	LANL (USA)	0–150 MeV (n)	CINDER90	Reactors, LANSCE
Geant4	CERN collab.	0–PeV	External	LHC, medical
MARS15	Fermilab (USA)	0.1 eV–100 TeV	Built-in	Fermilab complex
ActiWiz	CERN	N/A	Full chain	CERN waste class.

Modern approaches typically employ a two-step process: (i) a Monte Carlo transport calculation to determine the particle fluence spectra at each location of interest; and (ii) a dedicated activation/decay code that folds the fluence spectra with the relevant cross-section libraries to compute the radionuclide inventory as a function of irradiation and cooling time. FLUKA incorporates both steps internally through its built-in activation module, making it particularly convenient for accelerator applications [34,35]. PHITS uses the DCHAIN-SP code for the activation step, while MCNP6 couples with CINDER90 [36].

The CERN-developed ActiWiz tool [38] automates the activation and waste classification workflow by combining pre-computed FLUKA libraries with the full Bateman equation solver, enabling rapid parametric studies of material selection and operational scenarios. It has been validated against gamma spectrometry measurements of activated components from the LHC and SPS [35,38].

Mitigation Strategies and Decommissioning Considerations

The most effective strategy for minimizing induced radioactivity is the selection of materials that produce only short-lived activation products. Aluminum alloys and graphite are preferred over steel and copper where structural requirements allow, because their activation products (principally ^{11}C, ^{22}Na, ^{24}Na) have much shorter half-lives than ^{60}Co and ^{54}Mn produced in steel and iron [2,11]. For concrete, the use of low-activation aggregates with controlled trace element content (Eu < 0.1 ppm, Co < 1 ppm) can reduce long-term dose rates by up to an order of magnitude [18–20].

Minimizing beam losses through improved beam optics and collimation directly reduces activation. At modern proton synchrotrons, controlled beam losses are localized in dedicated collimation regions equipped with removable absorbers, allowing activated material to be handled separately [39]. Adequate ventilation of accelerator enclosures (typically 3–10 air changes per hour) maintains airborne radionuclide concentrations well below derived air concentration (DAC) limits [1,23]. Cooling water systems incorporate mixed-bed ion-exchange resins and delayed-release tanks to manage waterborne radioactivity [21].

At the end of facility life, activated materials must be characterized and classified for disposal. The waste classification depends on the specific activity of individual nuclides and is typically defined by national regulations (e.g., NRC 10 CFR 61 in the USA, or EU Directive 2013/59/Euratom). The key long-lived nuclides determining waste class are ^{60}Co, ^{152}Eu, ^{154}Eu, ^{134}Cs, and ^{36}Cl. Accurate prediction of these inventories using Monte Carlo methods is essential for decommissioning cost estimation and scheduling [18,38,40,41].

Conclusion. Induced radioactivity is an inherent consequence of operating particle accelerators and requires careful management throughout the facility lifecycle. This review has presented a systematic analysis of the principal sources of induced radioactivity, covering accelerator structural components, concrete shielding, cooling water, air, soil, and groundwater. The main conclusions are:

(1) Neutrons are the dominant agent of activation. The radionuclide inventory depends strongly on the neutron energy spectrum, which determines whether thermal capture, threshold reactions, or spallation dominate. Materials with higher atomic number produce a larger variety of longer-lived activation products.

(2) In structural materials, ^{60}Co, ^{54}Mn, and ^{65}Zn are the principal contributors to residual dose rates during maintenance periods. Material selection (graphite or aluminum over steel/copper where possible) is the most effective mitigation strategy.

(3) In concrete shielding, trace elements (Eu, Co, Cs, Ba) dominate the long-term activation and waste classification. Low-activation concrete formulations can reduce decommissioning costs substantially.

(4) Tritium is the critical radionuclide in both cooling water and groundwater, as it cannot be removed by conventional treatment and migrates at the velocity of natural water flow.

(5) Air activation is managed effectively by ventilation systems, with ^{11}C, ^{13}N, ^{15}O, and ^{41}Ar being the principal contributors to occupational doses.

(6) Monte Carlo codes, particularly FLUKA and PHITS, have reached a level of maturity where activation predictions agree with measurements to within a factor of 2–3 for most scenarios, enabling reliable facility design and decommissioning planning.

Future challenges include the management of activation at next-generation high-intensity facilities (ESS, FAIR, ILC), where beam powers of several MW will produce unprecedented levels of induced radioactivity. Advances in machine learning-assisted optimization of material selection and shielding design, combined with improved nuclear data libraries in the 100–1000 MeV range, will be essential for meeting these challenges.

References

1. Thomas, R.H., Patterson, W.H., Accelerator Health Physics, Academic Press, New York (1973).
2. NCRP, Radiation Protection for Particle Accelerator Facilities, NCRP Report No. 144, Bethesda, MD (2003).
3. Stevenson, G.R., Induced activity in accelerator structures, air and water, Radiat. Prot. Dosim. 96 (2001) 373–380.
4. Böhlen, T.T. et al., The FLUKA Code: developments and challenges for high-energy and medical applications, Nucl. Data Sheets 120 (2014) 211–214.
5. Battistoni, G. et al., Overview of the FLUKA code, Ann. Nucl. Energy 82 (2015) 10–18.
6. Sullivan, A.H., A Guide to Radiation and Radioactivity Levels Near High Energy Particle Accelerators, Nuclear Technology Publishing, Ashford (1992).
7. Swanson, W.P., Radiological safety aspects of electron linear accelerators, IAEA Technical Report Series No. 188, Vienna (1979).
8. Kase, K.R., Bjarngard, B.E., Attix, F.H. (Eds.), The Dosimetry of Ionizing Radiation, Vol. III, Academic Press, New York (1990).
9. Barbagallo, M. et al., High-accuracy determination of the neutron flux at n_TOF, Eur. Phys. J. A 49 (2013) 156.
10. Michel, R. et al., Cross sections for production of residual nuclides by protons, Nucl. Instrum. Methods B 129 (1997) 153–193.
11. Bozzato, D. et al., Induced radioactivity in accelerator materials studied at CERN CHARM facility, Radiat. Phys. Chem. 236 (2025) 112879.
12. Yu, Y. et al., Study on induced radioactivity in proton therapy accelerators using FLUKA, Radiat. Phys. Chem. 2024, 111751.

13. Yu, Y. et al., Induced radioactivity assessment in proton therapy rooms, J. Radiat. Prot. Res. 50 (2025).
14. Nakao, N. et al., Benchmark experiments on neutron shielding and activation in accelerator facilities, Radiat. Prot. Dosim. (2024).
15. Yang, Y. et al., Shielding and activation performance of concrete in carbon-ion therapy facilities, Radiat. Phys. Chem. (2024).
16. Barbhuiya, S. et al., Radiation shielding concrete: properties and activation considerations — a review, Struct. Concr. (2025).
17. Brugger, M. et al., Benchmark studies of induced radioactivity at CERN, Prog. Nucl. Sci. Technol. 4 (2014) 318–322.
18. Nakashima, H. et al., Low-activation concrete design for J-PARC, J. Nucl. Sci. Technol. 41 (2004) 7–12.
19. Zanini, L. et al., Shielding aspects of the ESS target station, Nucl. Instrum. Methods B 562 (2024) 165351.
20. Rindi, A., Measurement of ^{7}Be produced in water by 600 MeV protons, LNF Report (1972).
21. Yang, B., Induced Radioactivity at High-Intensity Heavy-Ion Accelerators, PhD Thesis, UCAS (2023).
22. Swanson, W.P., Thomas, R.H., Air activation in accelerators, in: Dosimetry of Ionizing Radiation, Vol. III (1990).
23. Butala, S.W., Baker, S.I., Yurista, P.M., Airborne radionuclides at proton accelerators, Health Phys. 57 (1989) 909–916.
24. Vincke, H., Theis, C., ActiWiz radiation protection tool, CERN Courier 52(6) (2012) 21–23.
25. ICRP, Human Respiratory Tract Model, Publication 66 (1994).
26. Endo, A., Yamaguchi, Y., Dose coefficients for radionuclide intake, JAERI (1999).
27. Borak, T.B. et al., Migration of radionuclides near proton accelerators, Health Phys. 23 (1972) 679–687.
28. Rokni, S., Liu, J.C., Roesler, S., Soil activation near NLC beamlines, Proc. SATIF-5 (2000).
29. Miura, T. et al., Soil contamination around KEK accelerator, J. Radioanal. Nucl. Chem. 255 (2003) 543–548.
30. Magistris, M., Onal, F., Environmental radioactivity at CERN, CERN-RP-2018-001 (2018).
31. Baker, S.I. et al., Leaching of accelerator radionuclides, Health Phys. 73 (1997) 912–918.
32. U.S. DOE, Radiation Protection of the Public and Environment, DOE Order 458.1 (2011).
33. Sato, T. et al., PHITS version 3.02, J. Nucl. Sci. Technol. 55 (2018) 684–690.
34. Agostinelli, S. et al., GEANT4 simulation toolkit, Nucl. Instrum. Methods A 506 (2003) 250–303.
35. Iwamoto, Y., Tsuda, S., Ogawa, T., Benchmark shielding calculations for fusion and accelerator-driven sub-critical systems. Frontiers in Energy Research. 11 (2023)1085264.
36. Nakao, N. et al., Activation benchmarks at CHARM mixed-field facility, CERN Report (2023).
37. Assmann, R.W. et al., Final collimation system for the LHC, Proc. EPAC (2006).
38. Ferrari, M., Alía, R. G., Giles, T., Senajova, D., Pandini, S., Zenoni, A., & Calviani, M. "Radiation to Materials" at CERN. IEEE Transactions on Nuclear Science, 70(8) (2023). 1580-1586.
39. Garini, G., Magni, C., Postuma, I., Fatemi, S., Ramos, R., Marcaccio, B., ... & Bortolussi, S. (2025). Evaluation of patient activation and dosimetry after Boron Neutron Capture Therapy. arXiv preprint arXiv:2501.13053.
40. Khasanov, Sh. et al., Induced radioactivity at particle accelerators: a short review, Radiat. Detect. Technol. Methods 5 (2021) 481–492.

SAMARQAND DAVLAT UNIVERSITETI ILMIY AXBOROTNOMASI

НАУЧНЫЙ ВЕСТНИК SCIENTIFIC REPORTS

Texnik muharrir **Sh.Xoliqulov**

Muharrirlar:

I.Sulaymonov - fil.f.d., dotsent
E.Arziqulov - f.-m.f.d., dotsent
O.Yusupova - fil.f.n., dotsent

Mas'ul muharrir:

A. Sh. Yarmuxamedov - f.-m.f.n.

Muassis: Samarqand davlat universiteti Manzil: 140104,
Samarqand shahri, Universitet xiyoboni, 15.
Telefon: (0 366) 240-38-47, Faks: (0 366) 239-13-87 e-mail:
axborotnoma.uz
SamDU «Ilmiy axborotnoma» jurnali tahririyati kompyuterida terildi. Bosishga 30.03.2026-yilda ruxsat etildi. Qog'oz o'lchami A-4. Nashriyot hisob tabog'i 10,00
Buyurtma raqami 833. Adadi 30 nusxa.

ISSN 2181-1296